Biophysical Journal
Article

Biophysical Society

Ancestral Interactions of Ribosomal RNA and Ribosomal Proteins

Kathryn A. Lanier,[1] Poorna Roy,[1] Dana M. Schneider,[1] and Loren Dean Williams[1,*]
[1]School of Chemistry and Biochemistry, Georgia Institute of Technology, Atlanta, Georgia

ABSTRACT We have proposed that the ancient ribosome increased in size during early evolution by addition of small folding-competent RNAs. In this Accretion Model, small RNAs and peptides were subsumed onto subunit surfaces, gradually encasing and freezing previously acquired components. The model predicts that appropriate rRNA fragments have inherited local autonomy of folding and local autonomy of assembly with ribosomal proteins (rProteins), and that the rProtein and rRNA are co-chaperones. To test these predictions, we investigate the rRNA interactions of rProtein uL23 and its tail, $uL23^{tail}$, which is a β-hairpin that penetrates deep into the core of the large ribosomal subunit. In the assembled ribosome, $uL23^{tail}$ associates with Domain III of the rRNA and a subdomain called "$DIII^{core}$". Here using band shift assays, fluorescence Job plots, and yeast three-hybrid assays, we investigate the interactions of rProtein uL23 and its tail with Domain III and with $DIII^{core}$ rRNA. We observe $rRNA_1$-$uL23^{tail}{}_1$ complexes in the absence of Mg^{2+} ions and $rRNA_1$-$uL23^{tail}{}_n$ ($n > 1$) complexes in the presence of Mg^{2+} ions. By contrast, the intact uL23 rProtein binds in slightly anticooperative complexes of various stoichiometries. The globular and tail regions of rProtein uL23 are distinctive in their folding behaviors and the ion dependences of their association with rRNA. For the globular region of the rProtein, folding is independent of rRNA, and rRNA association is predominantly by nonelectrostatic mechanisms. For the tail region of the protein, folding requires rRNA, and association is predominantly by electrostatic mechanisms. We believe these protein capabilities could have roots in ancient evolution and could be mechanistically important in co-chaperoning the assembly of the ribosome.

INTRODUCTION

The ribosome is responsible for synthesis of all coded proteins in all organisms. Ribosomal RNAs (rRNAs) catalyze decoding and peptidyl transfer (1–3), whereas ribosomal proteins (rProteins) stabilize and rigidify rRNAs. The cores of ribosomal particles are penetrated by rProtein tails (rTails) that extend inward from globular domains residing on subunit surfaces. rTails contain elongated and idiosyncratic polypeptide conformations and isolated secondary structural elements. The ribosome surface is a patchwork of rRNA and globular proteins.

It is remarkable, considering its size, complexity, asymmetry, and molecular precision that assembly of the bacterial ribosome is highly robust and flexible and can occur by a variety of parallel pathways (4). Transcription and folding of rRNA, translation and folding of rProteins, and rRNA-rProtein assembly occur in concert (5). The small ribosomal subunit contains 21 rProteins and the 16S rRNA, whereas the large ribosomal subunit (LSU) contains 33 rProteins and the 23S and 5S rRNAs.

We have recently proposed the Accretion Model of ribosomal evolution (6–8), in which the ancestral ribosome grew by recursive accumulation of oligomers of peptide and RNA onto subunit surfaces, encasing and freezing previously acquired components. The addition of new fragments onto subunit surfaces left the previous core unperturbed. During accretion, the folding of short rRNAs and polypeptides into secondary and tertiary structures were emergent phenomena, dependent on rRNA-rPeptide interactions (8,9).

The Accretion Model makes specific predictions about the folding and co-assembly of rRNA and rProteins. The model predicts that rRNA and rProtein segments have inherited chaperone functions in which small rRNA segments catalyze rProtein folding and rProteins catalyze rRNA assembly. These chaperone functions require both native and non-native interactions between rProtein and rRNA during folding and assembly, in funnel-like processes.

To investigate predictions of the Accretion Model, we characterize interactions of intact rProtein uL23 or its isolated rTail with rRNA partners as indicated by the assembled ribosome. We determine that the rProtein associates with rRNA via a subtle balance of native and non-native interactions.

Submitted January 23, 2017, and accepted for publication April 6, 2017.

*Correspondence: loren.williams@chemistry.gatech.edu

Editor: Tamar Schlick.

http://dx.doi.org/10.1016/j.bpj.2017.04.007

We have previously shown that isolated rRNA domains and subdomains fold to native-like structures (10,11).

Here we investigate isolated rRNA Domain III, its subdomain (DIII^{core}), rProtein uL23, and its rTail (uL23^{tail}). In the native ribosome, uL23^{tail} penetrates the LSU, and interacts with DIII^{core} (Fig. 1). We cleaved uL23^{tail} from the globular domain of rProtein uL23, and experimentally assayed binding of intact rProtein uL23 and isolated uL23^{tail} with Domain III and DIII^{core} in vitro and in vivo. We have investigated in vitro binding with fluorescence and band shift assays and in vivo binding with the yeast three-hybrid assay. We parsed the molecular interactions between the rRNA and the rProtein, and between the rRNA and the rTail, and qualitatively determined effects of electrostatic contributions of the interactions.

MATERIALS AND METHODS

Geometric analysis of molecular interactions

rRNA-rPeptide interactions were characterized by inspection of the three-dimensional structure of the *Thermus thermophilus* 70S ribosome (PDB: 1VY4) (12) and from FR3D (13). Coordinates of Domain III rRNA were extracted from the intact ribosomal structure. rRNA-rProtein interaction geometries were obtained directly from the crystal structure; rRNA within 3.4 Å of any atom of uL23 was defined as "contacted". Coulombic interactions were defined at a cutoff distance of 5.5 Å between a NH_3^+ of lysine or arginine R-groups and a phosphate group of the rRNA backbone. Hydrogen bonds were identified when an appropriate hydrogen bond donor was located within 3.4 Å of a hydrogen bond acceptor. Cation-π interactions were defined by a cutoff distance of 6.0 Å and a cutoff angle of 60° between the normal to the plane of the π-system and the vector connecting the center of the π-system of a nucleobase to the NH_3^+ of an amino acid side chain (14).

DIII^{core} rRNA sequence

DIII^{core} is composed of two fragments of rRNA. To transform DIII^{core} into a single continuous polymer, we joined the two fragments of rRNA together with a stem-loop as described in Lanier et al. (10). This linkage was designed to leave the DIII^{core} structure unperturbed. The termini of the two DIII^{core} fragments form a double-stranded A-form helical arm (Helix 54) that can dock onto the stem-loop without perturbation. The linkage (5′-gccGUAAggc-3′) is a GNRA stem-loop (15) on a three-basepair helical stem (Fig. S1).

Continuous variation

The uL23^{tail}, comprising amino acids His^{58}–Ala^{79} with addition of Trp^{80} (HV**RGKKKR**LG**R**YLG**KR**PD**RKK**AW, the 11-cationic amino acids are *bold*), was purchased from RS Synthesis (Louisville, KY). We added a tryptophan to the C-terminus of uL23^{tail}, where a tryptophan is observed in uL23 of *Escherichia coli*. Maintaining a constant total concentration of rRNA and uL23^{tail}, the mole fraction of uL23^{tail} to rRNA was varied. The concentration of uL23^{tail} was evaluated after peptide hydrolysis (16). uL23^{tail} was hydrolyzed in 6 M HCl at 150°C for 6 h in Pierce Vacuum Hydrolysis Tubes (Rockford, IL). After hydrolysis, the sample was concentrated by removing the hydrochloric acid with a stream of argon. The absorbance of tryptophan in the hydrolyzed sample was measured at 278 nm.

The rRNA and uL23^{tail} were suspended in 10 μL of 20 mM Tris-HCl, pH 8.3, heated to 85°C for 30 s, then cooled to 30°C at a rate of 1.5°C/min. Fluorescence emission of Trp^{80} was monitored at 350 nm using a BioTek Synergy H4 Multi-Mode Plate Reader (Winooski, VT). The fluorescence of Trp^{80} is quenched by association with Domain III or DIII^{core} rRNA.

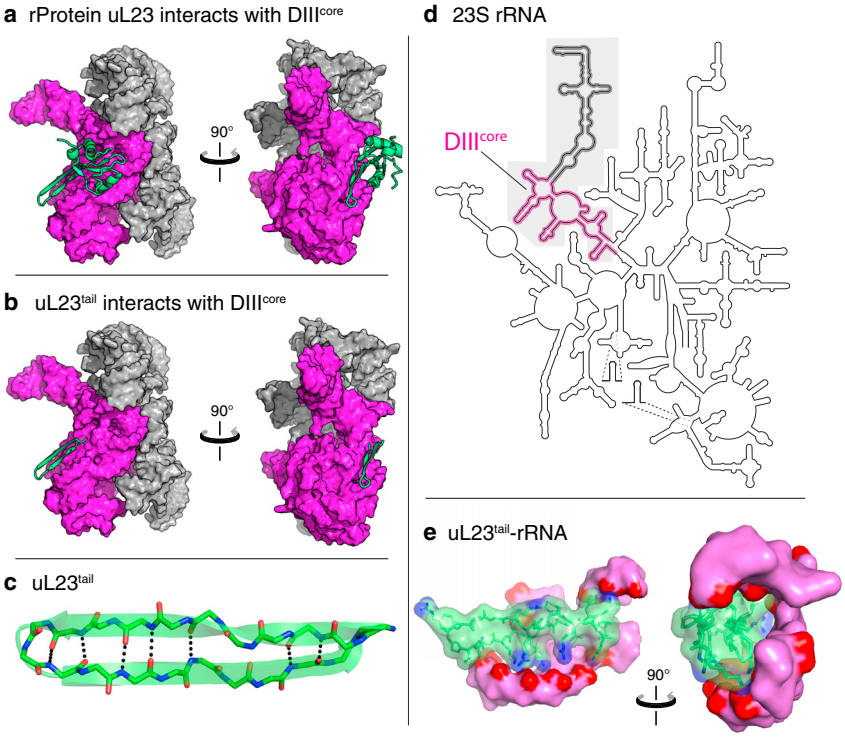

FIGURE 1 Domain III rRNA and rProtein uL23 as observed in the native ribosome. (*a*) DIII^{core} (*magenta*) interacts with rProtein uL23 (*green*). The remainder of Domain III is gray. (*b*) uL23^{tail} (*green*) forms a β-hairpin that traverses the surface of DIII^{core}. (*c*) Shown here is a cartoon representation of the β-hairpin structure of uL23^{tail}. Hydrogen bonds are shown as dashed lines. (*d*) Shown here is the secondary structure of the LSU rRNA highlighting Domain III (*gray box*) and DIII^{core} (*magenta line*). (*e*) The rRNA wraps around uL23^{tail}, forming a pocket that is complementary to the folded peptide. The anionic phosphate oxygens of the rRNA are red. Cationic nitrogens of uL23^{tail} are blue. Coordinates are from the *T. thermophilus* ribosomal structure (PDB: 1VY4; (12)). To see this figure in color, go online.

Electrophoretic mobility shift assay experiments

Solutions of 10 μM in vitro-transcribed Domain III or DIII^{core} were prepared in 100 mM NaCl, 20 mM Tris-HCl, pH 8.0 buffer. For experiments with Mg^{2+}, $MgCl_2$ was added to a 5 mM final concentration. rRNA solutions were annealed by heating to 85°C for 30 s then cooling at a linear rate of 1.5°C/min to 30°C. Binding reactions of 10 μL (100 mM NaCl, 20 mM Tris-HCl, pH 8.0) with and without Mg^{2+} were conducted with 1 μM annealed Domain III or DIII^{core}. Construction and purification of fusions of Maltose Binding Protein (MBP) with uL23^{tail} and intact uL23 rProtein are described in the Supporting Material. uL23-MBP or uL23^{tail}-MBP was added to aliquots of the rRNA solution to give protein concentrations ranging from 0.5 to 10 μM. Solutions were incubated at room temperature for 30 min. Glycerol was added to a final concentration of 10% immediately before loading onto a 5% nondenaturing polyacrylamide (29:1 (w/w) acrylamide/bisacrylamide, 3% glycerol, 0.5× TBE) gel. The gels were prerun for 60 min, and electrophoresis was conducted at 120 V for 45–60 min. After the completion of electrophoresis, the gel was stained sequentially with fluorescent dyes, SYBR Green II and SUPRO Red, using a two-color fluorescence dye protocol (17). After staining, the gels were visualized on a transilluminator.

Yeast three-hybrid assay

In yeast strain YBZ-1, the *HIS3* reporter gene is under the control of the LexA operator. Hybrid 1, a LexA/MS2 coat protein fusion, binds to the LexA operator. The MS2 coat protein domain binds tightly to the MS2 sequence of the hybrid RNA, which contains the MS2 RNA and the rRNA sequence of interest (e.g., Domain III or DIII^{core}). In Hybrid 3, the protein of interest (e.g., rProtein uL23) is fused to the yeast GAL4 transcriptional activation domain (GAD). In vivo RNA-protein binding completes Hybrid 2, resulting in expression of the *HIS3* reporter gene. The strength of rRNA-rProtein binding was determined by resistance to 3-Amino-1,2,4-triazole (3-AT), a competitive inhibitor of the *HIS3* gene product, imidazoleglycerol-phosphate dehydratase.

Yeast three-hybrid assays were performed in the YBZ-1 yeast strain as described in Hook et al. (18). Double transformants were selected in a medium lacking adenine and leucine (CM-AL), and subsequently grown in media lacking adenine, leucine, and histidine (CM-ALH) with 0.0, 0.1, 0.2, 0.3, and 0.4 mM 3-AT. Interactions between Domain III or DIII^{core} rRNA and rProtein uL23 result in activation of the GAL4 promoter and *HIS3* gene transcription and are quantitatively evidenced by growth in CM-ALH media. *HIS3* activity in this assay correlates with RNA-protein affinity as measured in vitro over a 10-fold to 100-fold range (18). The positive control was RNA aptamer p50-MS2 and GAD-p53 (19). Negative controls included assays of each protein hybrid with only the MS2 RNA (T-cassette vector without insert). Additional negative controls included the RNA-hybrid with GAD (pACTII vector without insert), the RNA-hybrid alone, and the protein-hybrid alone (data not shown). Culture growth was determined by optical density at 630 nm.

RESULTS

Molecular interactions of DIII^{core} with rProtein uL23

Using the three-dimensional structure, we parsed the molecular interactions (Coulombic, cation-π and hydrogen bonding) that link DIII^{core} rRNA to rProtein uL23 in the native structure of the LSU. As noted previously (20), rProtein uL23 interacts Coulombically with DIII^{core}; positively charged functional groups of several lysines are in close proximity to negatively charged phosphate groups of the rRNA (Fig. 1 *e*). These electrostatic interactions are observed for K16-U1340 (NZ-O1P: 2.7 Å), K40-A1596 (NZ-O1P: 5.0 Å), K40-A1597 (NZ-O2P: 3.9 Å), K62-U1312 (NZ-O2P: 3.3 Å), and K77-U1340 (NZ-O1P: 3.7 Å). Hydrogen bonds are observed between K16 and U1340 (2.7 Å) and between K78 and U1341 (2.8 Å). Two cation-π interactions (defined by a cutoff distance of 6.0 Å and a cutoff angle of 60°) (14,21,22) are observed between cationic amino acids of rProtein uL23 and the aromatic systems of bases in DIII^{core}; K16 interacts with A1393 (5.7 Å) and K77 interacts with U1341 (3.3 Å). The structure indicates that when uL23^{tail} is folded into a β-hairpin, cationic amino acid side chains of uL23^{tail} and anionic phosphate groups of the rRNA form complementary arrays.

The amino acids of rProtein uL23 that interact with DIII^{core} rRNA in the intact ribosome are highly conserved over phylogeny. Alignments of uL23 sequences from a subset of 121 organisms in a sparse representation of the three domains of life (7) reveal five cationic amino acids K16, K40, K62, K77, and K78 that are highly conserved (present in >90% of the sequences sampled, Supporting Material). All conserved amino acids of rProtein uL23 interact exclusively with DIII^{core} rRNA.

rRNA-rProtein and rRNA-rPeptide stoichiometry

Continuous variation suggests uL23^{tail} forms near 1:1 complexes with Domain III and with DIII^{core}

We characterized stoichiometries of the interaction of uL23^{tail} with Domain III and with DIII^{core} in vitro in the absence and presence of Mg^{2+} using a spectroscopic assay and the method of continuous variation (23,24). A series of solutions with varying ratios of uL23^{tail} to rRNA were prepared with a constant total volume. To enable detection of rRNA-rPeptide interaction by fluorescence, we added a tryptophan to the C-terminus of uL23^{tail}. A tryptophan is present at this position in the *E. coli* rProtein uL23, but not in the *T. thermophilus* uL23.

We inferred stoichiometries of binding from the discontinuities in plots of fluorescence intensity versus mole fraction of uL23^{tail} and rRNA. The results suggest that in the absence of Mg^{2+}, uL23^{tail} predominantly forms complexes with an average near 1:1 stoichiometry (rRNA$_1$-uL23$^{tail}_1$). This behavior is observed with both Domain III and with DIII^{core} (Fig. 2, *a* and *b*). A complex with 1:1 stoichiometry would give a discontinuity at mole fraction 0.5. Discontinuities are observed at mole fraction 0.55 for Domain III and 0.54 for DIII^{core}. Upon the addition of 10 mM Mg^{2+}, the discontinuity shifts to the right (towards a greater ratio of uL23^{tail} to rRNA; Fig. 2, *c* and *d*). In the presence of Mg^{2+}, discontinuities are observed at mole fraction 0.71 for Domain III and 0.62 for DIII^{core}. This direction of shift in the discontinuity away from mole fraction 0.5 is reproducible, suggesting increased formation of rRNA$_1$-uL23$^{tail}_n$

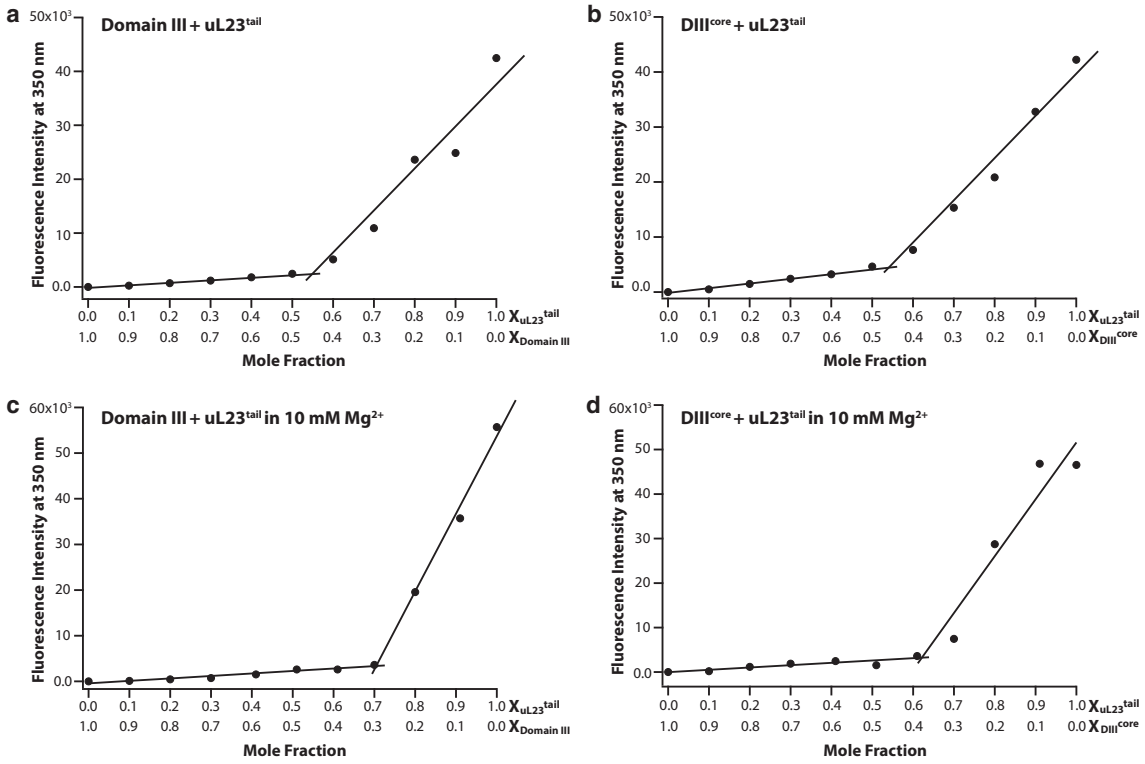

FIGURE 2 Continuous variation of fluorescence intensity versus mole fraction (X) of uL23^{tail} and Domain III or DIII^{core} rRNAs. (*a*) and (*b*) represent binding in the absence of divalent cations, whereas (*c*) and (*d*) represent binding in the presence of 10 mM Mg^{2+}. In the absence of Mg^{2+} the best-fit lines intersect at uL23^{tail} mole fraction (*a*) $x = 0.55$ for Domain III and (*b*) at $x = 0.54$ for DIII^{core}, each suggesting 1:1 stoichiometry of interaction of uL23^{tail} with Domain III or DIII^{core} rRNAs. (*c*) In the presence of Mg^{2+}, the best-fit lines intersect at $x = 0.71$ for Domain III and (*d*) at $x = 0.62$ for DIII^{core}. The fluorescence emission was monitored at 350 nm.

complexes with $n > 1$. The data are most consistent with a model in which uL23^{tail} forms rRNA$_1$-uL23$^{tail}_n$ complexes with $n > 1$ with both Domain III and with DIII^{core} in the presence of Mg^{2+}. The close similarities in the Job plots for uL23^{tail} with both Domain III and with DIII^{core} suggest that uL23^{tail} interacts primarily with the DIII^{core} region of Domain III and not with regions of Domain III outside of DIII^{core}. Control experiments with *Tetrahymena thermophila* Group I intron P4–P6 RNA are consistent with less-specific binding with uL23^{tail}, and are without a clear inflection point (Fig. S2).

Electrophoretic mobility shift assay confirms binding of uL23^{tail} with Domain III and with DIII^{core} in vitro

Two-color electrophoretic mobility shift assays (EMSAs) (17) were used to evaluate binding affinities and stoichiometries of rProtein uL23 or uL23^{tail} with Domain III or DIII^{core}. In the two-color EMSAs, free RNA appears as a green band on the gel and free protein as a red band. RNA-protein complexes produce a colocalized yellow band (Figs. 3 and 4). MBP was fused to the N-terminal of uL23^{tail} and intact rProtein uL23 to induce changes in mobility of the rRNA upon complex formation. Control experiments in which Domain III and DIII^{core} rRNAs were incubated with MBP lacking the uL23 or uL23^{tail} fusion demonstrate that MBP does not form complexes with Domain III or DIII^{core} rRNAs.

Binding reactions were performed in both the absence (Fig. 3, *a* and *b*) and presence of Mg^{2+} (Fig. 3, *c* and *d*). In both types of experiments, Domain III and DIII^{core} associate with uL23^{tail} as indicated by changes in mobility and red and green colocalization, giving a yellow band (Fig. 3).

The mobilities of the rRNA-uL23^{tail} complexes decrease continuously with increasing peptide concentration. This observation is consistent with dynamical phenomena, in which the rPeptide dissociates/associates from the rRNA during electrophoresis (25). By mass action, higher concentration of rPeptide would push the rRNA towards the fully associated state. Stoichiometries of uL23^{tail} and rRNA in these EMSA experiments would be difficult to infer because of averaging and dynamics during the experiment.

Relative dissociation constants (K_d values) were crudely estimated by fitting the EMSA data to a simple binding model, assuming a stoichiometry of 1:1. Concentrations of various species in the binding reaction between uL23^{tail} and Domain III or DIII^{core} were obtained by integrating the band intensities on the EMSA gels. The apparent K_d for uL23^{tail} in association with Domain III is estimated to be 2.8 μM in the absence Mg^{2+} and 4.4 μM in the presence

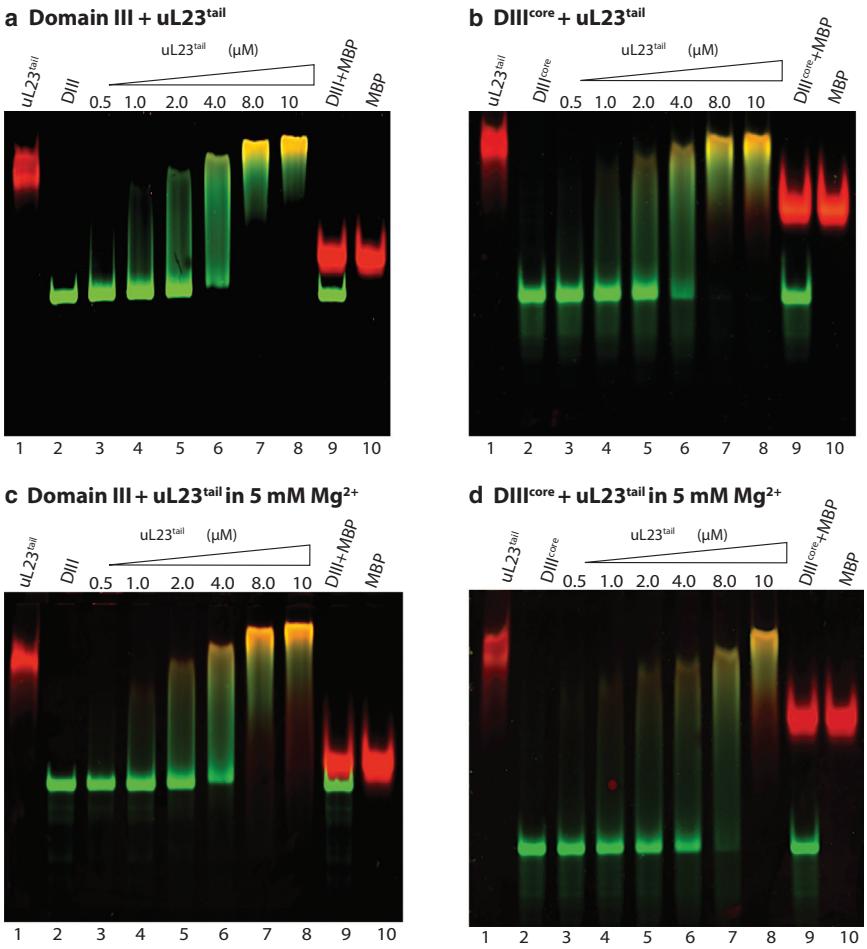

FIGURE 3 Mobility shift assays of uL23^{tail} in association with Domain III or DIII^{core}. rRNA, rPeptide, and rRNA-rPeptide complexes were visualized on 5% native-PAGE gels by two-color EMSA. Binding reactions were performed with 1 μM rRNA in 100 mM NaCl, 20 mM Tris-HCl, pH 8.0. The [rRNA]:[rPeptide] ratios are indicated above the lanes. All gels show uL23^{tail} alone (*lane 1*), rRNA alone (*lane 2*), and MBP controls (*lanes 9 and 10*). MBP alone shows no interaction with rRNA (*lane 9*). (*a*) Shown here is Domain III with uL23^{tail} (*lanes 3–8*). (*b*) Shown here is DIII^{core} with uL23^{tail} (*lanes 3–8*). (*c*) Shown here is Domain III with uL23^{tail} (*lanes 3–8*) under the same conditions as (*a*), except with the addition of 5 mM Mg^{2+}. (*d*) Shown here is DIII^{core} with uL23^{tail} (*lanes 3–8*) under the same conditions as (*b*), except with the addition of 5 mM Mg^{2+}. To see this figure in color, go online.

of Mg^{2+}. The apparent K_d for uL23^{tail} in association with DIII^{core} is estimated to be 3.0 μM in the absence of Mg^{2+} and 5.3 μM in the presence of Mg^{2+}. For both of these complexes, the affinity of the rPeptide for the rRNA appears to be attenuated by Mg^{2+}, suggesting that electrostatic interactions are a significant component of the binding interactions. Polyelectrolyte theory predicts this decrease in affinity with increasing salt concentration (26).

EMSA suggests rProtein uL23 forms noncooperative non-stoichiometric complexes with Domain III and with DIII^{core} in vitro

Similar to uL23^{tail}, full-length rProtein uL23 forms complexes with Domain III and with DIII^{core}, as indicated by shifts on the EMSA gels. In contrast to uL23^{tail}, rProtein uL23 associates with Domain III and with DIII^{core} to give distinct ladders (Fig. 4). In the simplest interpretation, this banding pattern indicates formation of multiple RP_n complexes (R = rRNA, P = rProtein, and n = number of rProtein molecules bound per rRNA molecule) (25). The ladder shifts to lower mobility species as the rProtein concentration increases as expected by mass action. The regions of the gels showing the lowest mobility species provide information on the maximum number of rProtein molecules bound per rRNA molecule. Domain III binds over seven uL23 rProteins, whereas DIII^{core} binds a maximum of nine. The differential stoichiometry of interaction between Doman III and DIII^{core} suggests rProtein uL23 binds to regions of Domain III outside of DIII^{core}.

To determine affinities and degree of cooperativity, the EMSA data were quantitated and fit to binding models. Concentrations were estimated by integrating the band intensities on the gels. K_d values were estimated by fitting for each RP_n complex (where $n = 1, 2, 3, 4$; Table 1). For complexes with $n > 4$, errors in integrated intensities were too great to be useful for this purpose. A model in which four K_d values were constrained to a single value gave a significantly worse fit than a model with four different K_d values. The single K_d model gave larger error residuals (Figs. S3–S6). In the best fits, $K_{d4} > K_{d3} > K_{d2} > K_{d1}$. The fits suggest that binding is anticooperative, indicating that the affinity of the first rProtein for the rRNA is greater than that of the second rProtein, which is greater than that of the third, which is greater than that of the fourth. Neither addition of Mg^{2+} nor the conversion of Domain III to DIII^{core} changes the ranking of the K_d values.

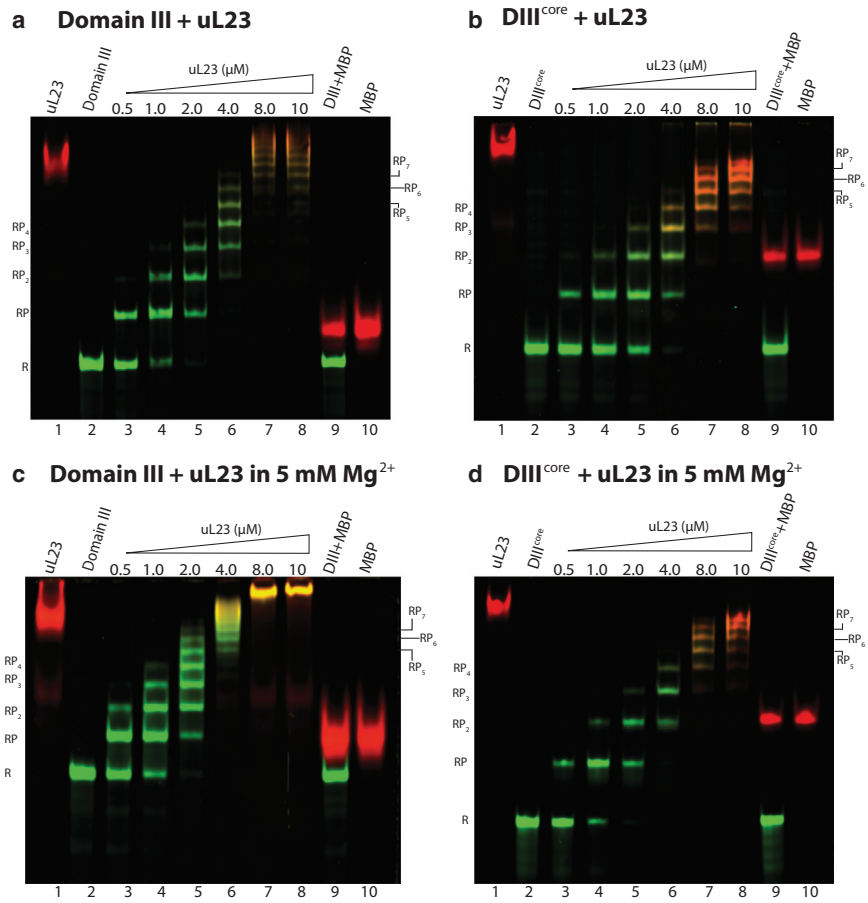

FIGURE 4 Mobility shift assays demonstrating that intact rProtein uL23 binds to multiple sites on Domain III and DIII^{core} rRNAs. All binding reactions were performed with 1 μM rRNA in 100 mM NaCl, 20 mM Tris-HCl, pH 8.0. The [rRNA]:[rProtein] ratios are indicated above the lanes. All gels show uL23 alone (*lane 1*), rRNA alone (*lane* 2), and MBP controls (*lanes 9 and 10*). MBP alone shows no interaction with Domain III or DIII^{core} (*lane 9*). (*a*) Shown here is Domain III with rProtein uL23 (*lanes 3–8*). (*b*) Shown here is DIII^{core} with rProtein uL23 (*lanes 3–8*). (*c*) Shown here is Domain III with rProtein uL23 (*lanes 3–8*) under the same conditions as (*a*), except with the addition of 5 mM Mg^{2+}. (*d*) Shown here is DIII^{core} with rProtein uL23 (*lanes 3–8*) under the same conditions as (*b*), except with the addition of 5 mM Mg^{2+}. To see this figure in color, go online.

The affinities of rProtein uL23 are uniformly greater for Domain III than for DIII^{core}. This difference is not altered by addition of Mg^{2+}. In contrast to observations with uL23^{tail}, Mg^{2+} increases the affinity of rProtein uL23 for the rRNA, for each RP_n complex. Therefore, for a given concentration of rRNA and rProtein, the addition of Mg^{2+} shifts the equilibrium condition to complexes of greater rProtein to rRNA ratio, consistent with observations in the Job plots. Because polyelectrolyte theory predicts the opposite (decreasing affinity with increasing salt concentration), it appears that nonelectrostatic interactions are important in the stabilization of these complexes.

TABLE 1 Dissociation Constants (K_d values) for Each Binding Site

	K_{d1} (μM)	K_{d2} (μM)	K_{d3} (μM)	K_{d4} (μM)
DIII-uL23	0.5	0.9	1.2	1.6
DIII^{core}-uL23	1.4	2.1	2.9	3.5
DIII-uL23, 5 mM Mg^{2+}	0.4	0.8	1.0	1.3
DIII^{core}-uL23, 5 mM Mg^{2+}	0.6	1.1	1.8	2.3

K_{d1} is the dissociation constant for the first binding site (RP_1), K_{d2} is the dissociation constant for the second binding site (RP_2), K_{d3} is the dissociation constant for the third binding site (RP_3), and K_{d4} is the dissociation constant for the fourth binding site (RP_4).

Domain III and DIII^{core} interact and associate with uL23 in vivo

We used the yeast three-hybrid system (18,27,28) to confirm interaction of Domain III and DIII^{core} with rProtein uL23 in vivo. In this system, association of bait RNA with prey protein in yeast increases expression of reporter gene *HIS3,* causing resistance to 3-AT (28). 3-AT is a competitive inhibitor of the *HIS3* gene product. Cells can survive only when the level of *HIS3* gene product is sufficient to overcome the inhibitory effect of a given level of 3-AT. Expression of the reporter gene produces sufficient histidine to allow cell survival. The level of 3-AT that confers lethality is a measure of the level of expression of *HIS3* and is therefore a measure of the strength of interaction between the bait RNA and the prey protein.

In the yeast three-hybrid assay, both Domain III and DIII^{core} are seen to interact with rProtein uL23 (Fig. 5). In vivo interaction of each rRNA with rProtein uL23 resulted in similar expression of reporter gene *HIS3*, as determined by resistance to 0.4 mM 3-AT. Although expression is less than that observed for the positive control (p50 RNA/p53 protein), it is well above that observed for the negative control (MS2 RNA/rProtein uL23 GAD) over a range of 3-AT concentrations. No expression was observed for the other negative

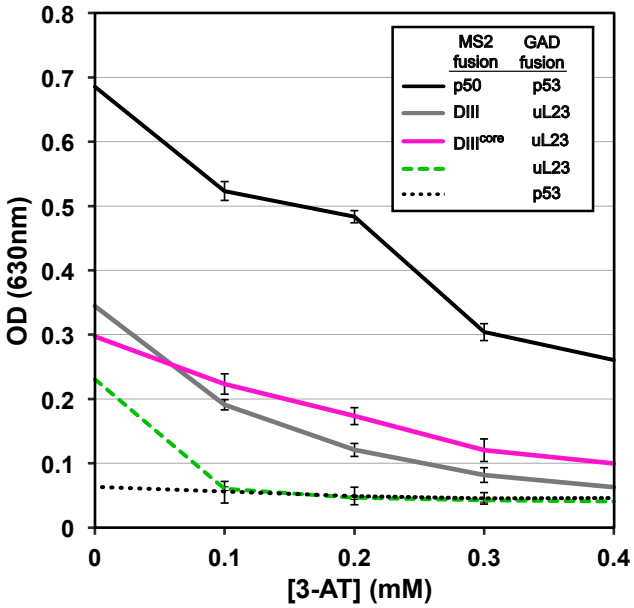

FIGURE 5 Yeast three-hybrid assay for interaction of Domain III or DIII^{core} with uL23. This plot shows the level of 3-AT resistance of yeast strain YBZ-1 expressing Domain III-MS2 or DIII^{core}-MS2 fusions and GAD-uL23 fusions. Cell growth (measured at optical density 630 nm after 48 h) is plotted against 3-AT concentration. Resistance to 3-AT indicates RNA-protein interaction. The positive control is p50-MS2 and GAD-p53. Negative controls (shown in *dashed lines*) are MS2 RNA alone (lacking Domain III or DIII^{core}) assayed with rProtein uL23 and p53. Activity from negative controls were used to determine the background signal. To see this figure in color, go online.

controls (RNA-hybrid with GAD, RNA-hybrid alone, and protein-hybrid alone).

DISCUSSION

The nature of the folding and assembly processes of the bacterial ribosome (4,5), including the robustness and flexibility, is consistent with an evolutionary model in which folding of rProtein and folding of rRNA were coemergent during development of the ribosome (8,9). In this model, folding of rRNA was emergent on interactions with polypeptide and folding of polypeptide was emergent on interactions with rRNA. This model predicts that rProtein and rRNA are co-chaperones. Their folding and assembly should be robust and flexible.

rProtein uL23 is located near the exit tunnel of the ribosome where it interacts with the trigger factor protein. The globular domain of this rProtein is on the surface of the LSU (29) and the extended segment that we call uL23^{tail} (Fig. 1) penetrates into the LSU. uL23^{tail} forms a β-hairpin that traverses the surface of DIII^{core} and penetrates well into the particle. For isolated uL23 in solution, the globular domain folds to the native state whereas the tail remains in random coil (30). Circular dichroism data show that in the absence of rRNA, uL23^{tail} is also in a random coil state (K.A.L. and L.D.W., unpublished data) as expected. Therefore, formation of a native-like complex of either uL23^{tail} or uL23 with DIII^{core} or Domain III would require folding to the β-hairpin observed in the assembled ribosome. Folding of uL23^{tail} to a β-hairpin allows specific geometric pairing of an array of cationic side chains of uL23^{tail} with negatively charged phosphate groups of the rRNA.

Intrinsic co-chaperone functions of rRNA and rProteins might require non-native interactions of folding and assembly intermediates. Here we determine whether uL23^{tail} or rProtein uL23 might bind to rRNA by non-native modes. We observe in EMSAs that isolated DIII^{core} and Domain III rRNAs associate with intact rProtein uL23. rProtein uL23 forms a series of well-resolved complexes with DIII^{core} and Domain III rRNAs, as can be seen on the EMSA gels. Intact uL23 associates with DIII^{core} and regions of Domain III outside of DIII^{core}. Association is also confirmed by yeast three-hybrid experiments, which do not provide information on stoichiometry or binding sites. However, the combined data suggest that rProtein uL23 forms non-native assemblies with rRNA. A variety of complexes appear to vary by stoichiometry (rRNA$_1$-uL23$_n$, n = 1, 2, 3, …) and are slightly anticooperative; each rProtein binds to a given rRNA fragment with less affinity than the previous rProtein. The affinities of rProtein uL23 for DIII^{core} and Domain III increase with increasing Mg^{2+} concentration. This ion dependence suggests that the predominant interactions between rProtein uL23 and the rRNA are nonelectrostatic in nature. Shorter range and more subtle interactions, such as hydrogen bonds, ion-dipole or dipole-dipole, must be important for these assemblies.

In contrast to rProtein uL23, the apparent affinities of uL23^{tail} for DIII^{core} and Domain III decrease with increasing Mg^{2+} concentration. In the absence of Mg^{2+} ions uL23^{tail} appears to form a 1:1 complex with Domain III and with DIII^{core} (rRNA$_1$- uL23$^{tail}_1$). Our structural analysis suggests that specific electrostatic interactions between rRNA phosphates and uL23^{tail} cationic amino acids drive folding of uL23^{tail} to a β-hairpin. Upon the addition of Mg^{2+} ions, the complexes switch from rRNA$_1$-uL23$^{tail}_1$ to rRNA$_1$- uL23$^{tail}_n$ stoichiometry (with $n > 1$). Formation of these complexes is indicated in the Job plots (Fig. 2). A change in binding mode is expected because Mg^{2+} would screen the electrostatic interactions and destabilize binding by the β-hairpin conformation of uL23^{tail}.

This ion dependence suggests that the predominant interactions between the β-hairpin form of uL23^{tail} and the rRNA are electrostatic in nature, consistent with our structural analysis. Complexes of rRNA$_1$-uL23$^{tail}_n$ ($n > 1$) cannot be excluded by EMSA because kinetic phenomena smear the gels.

In sum, the globular and tail regions of rProtein uL23 are distinctive in their folding behaviors and in the role of electrostatics in their interactions with rRNA. For the globular region of uL23, folding is independent of rRNA, and

association with rRNA is predominantly by nonelectrostatic mechanisms. For $uL23^{tail}$, folding requires rRNA, and association with the rRNA is predominantly by electrostatic mechanisms. We believe protein folding capabilities could have roots in ancient evolution and could be mechanistically important in co-chaperoning the assembly of the ribosome.

It appears that $uL23^{tail}$ is more ancient than the globular domain of uL23 (8). Their highly distinctive interactions with the rRNA are consistent with this model. It appears that in the intact rProtein, the binding preferences of $uL23^{tail}$ are overwhelmed by contributions from the globular domain of uL23. The effects of Mg^{2+} on $uL23^{tail}$ affinity and stoichiometry are obscured by the globular domain. In general, it can be said that the interactions of this rProtein with rRNA are complex and heteromorphous.

We previously constructed a 615-nucleotide biochemical model of the ancestral LSU rRNA derived from the 2787-nucleotide 23S rRNA of *T. thermophilus*, and showed that this rRNA folds and assembles with appropriate rPeptides (31). We also showed that the 367-nucleotide Domain III and the 199-nucleotide $DIII^{core}$ fold autonomously to a near-native states (10,11) when excised from the LSU.

Summary

We have proposed a model of ancient evolution of the ribosome, which selected for robustness in folding and assembly, and independence of small isolated components (7). Here, we isolate small rRNA and rProtein fragments, and assay them for folding and assembly. We have observed that rRNA fragments fold independently, and in this case the rRNA assembles with an ancient rProtein fragment. We observe ancestry-specific modes of interaction between the rProtein and the rRNA. It appears that rProteins are chimeras; the noncanonical tails are more ancient than the globular domains.

SUPPORTING MATERIAL

Supporting Materials and Methods, six figures, five tables, and one data file are available at http://www.biophysj.org/biophysj/supplemental/S0006-3495(17)30395-8.

AUTHOR CONTRIBUTIONS

K.A.L. performed experiments, contributed to experimental design, analyzed data, and collaborated with L.D.W. in writing the manuscript. L.D.W. contributed to experimental design and analyzed data. P.R. and D.M.S. performed experiments and analyzed data.

ACKNOWLEDGMENTS

We thank Marvin P. Wickens (University of Wisconsin-Madison) for providing us with the pACTII plasmid and James Maher for the providing us with the RNA hybrid p50-MS2 and protein hybrid GAD-p53 vectors.

This work was supported by NASA grant No. NNX16AJ29G.

REFERENCES

1. Ban, N., P. Nissen, …, T. A. Steitz. 2000. The complete atomic structure of the large ribosomal subunit at 2.4 A resolution. *Science.* 289:905–920.
2. Noller, H. F., V. Hoffarth, and L. Zimniak. 1992. Unusual resistance of peptidyl transferase to protein extraction procedures. *Science.* 256:1416–1419.
3. Selmer, M., C. M. Dunham, …, V. Ramakrishnan. 2006. Structure of the 70S ribosome complexed with mRNA and tRNA. *Science.* 313:1935–1942.
4. Davis, J. H., Y. Z. Tan, …, J. R. Williamson. 2016. Modular assembly of the bacterial large ribosomal subunit. *Cell.* 167:1610–1622. e1615.
5. Shajani, Z., M. T. Sykes, and J. R. Williamson. 2011. Assembly of bacterial ribosomes. *Annu. Rev. Biochem.* 80:501–526.
6. Petrov, A. S., B. Gulen, …, L. D. Williams. 2015. History of the ribosome and the origin of translation. *Proc. Natl. Acad. Sci. USA.* 112:15396–15401.
7. Petrov, A. S., C. R. Bernier, …, L. D. Williams. 2014. Evolution of the ribosome at atomic resolution. *Proc. Natl. Acad. Sci. USA.* 111:10251–10256.
8. Kovacs, N. A., A. S. Petrov, …, L. D. Williams. 2017. Frozen in time: the history of proteins. *Mol. Biol. Evol.* Published online Feb 15, 2017. http://dx.doi.org/10.1093/molbev/msx086.
9. Söding, J., and A. N. Lupas. 2003. More than the sum of their parts: on the evolution of proteins from peptides. *BioEssays.* 25:837–846.
10. Lanier, K. A., S. S. Athavale, …, L. D. Williams. 2016. Imprint of ancient evolution on rRNA folding. *Biochemistry.* 55:4603–4613.
11. Athavale, S. S., J. J. Gossett, …, L. D. Williams. 2012. Domain III of the *T. thermophilus* 23S rRNA folds independently to a near-native state. *RNA.* 18:752–758.
12. Polikanov, Y. S., T. A. Steitz, and C. A. Innis. 2014. A proton wire to couple aminoacyl-tRNA accommodation and peptide-bond formation on the ribosome. *Nat. Struct. Mol. Biol.* 21:787–793.
13. Sarver, M., C. L. Zirbel, …, N. B. Leontis. 2008. FR3D: finding local and composite recurrent structural motifs in RNA 3D structures. *J. Math. Biol.* 56:215–252.
14. Gallivan, J. P., and D. A. Dougherty. 1999. Cation-π interactions in structural biology. *Proc. Natl. Acad. Sci. USA.* 96:9459–9464.
15. Mohan, S., C. Hsiao, …, L. D. Williams. 2010. RNA tetraloop folding reveals tension between backbone restraints and molecular interactions. *J. Am. Chem. Soc.* 132:12679–12689.
16. Barkholt, V., and A. L. Jensen. 1989. Amino acid analysis: determination of cysteine plus half-cystine in proteins after hydrochloric acid hydrolysis with a disulfide compound as additive. *Anal. Biochem.* 177:318–322.
17. Shcherbakov, D., and W. Piendl. 2007. A novel view of gel-shifts: analysis of RNA-protein complexes using a two-color fluorescence dye procedure. *Electrophoresis.* 28:749–755.
18. Hook, B., D. Bernstein, …, M. Wickens. 2005. RNA-protein interactions in the yeast three-hybrid system: affinity, sensitivity, and enhanced library screening. *RNA.* 11:227–233.
19. Cassiday, L. A., and L. J. Maher, 3rd. 2001. In vivo recognition of an RNA aptamer by its transcription factor target. *Biochemistry.* 40:2433–2438.
20. Klein, D. J., P. B. Moore, and T. A. Steitz. 2004. The roles of ribosomal proteins in the structure assembly, and evolution of the large ribosomal subunit. *J. Mol. Biol.* 340:141–177.
21. Dougherty, D. A. 1997. Electrostatic models for the cation-π interaction and related non-covalent interactions. *J. Am. Chem. Soc.* 214:166.
22. Ma, J. C., and D. A. Dougherty. 1997. The cation-π interaction. *Chem. Rev.* 97:1303–1324.

23. Job, P. 1928. Studies on the formation of complex minerals in solution and on their stability. *Ann. Chim. Fr.* 9:113–203.

24. Cantor, C., and P. Schimmel. 1984. Biophysical Chemistry (I–III). Academic Press, New York.

25. Adams, C. A., and M. G. Fried. 2007. Analysis of protein-DNA equilibria by native gel electrophoresis. *In* Protein Interactions. P. Schuck, editor. Springer, Heidelberg, Germany, pp. 417–446.

26. Record, M. T., Jr., W. Zhang, and C. F. Anderson. 1998. Analysis of effects of salts and uncharged solutes on protein and nucleic acid equilibria and processes: a practical guide to recognizing and interpreting polyelectrolyte effects, Hofmeister effects, and osmotic effects of salts. *Adv. Protein Chem.* 51:281–353.

27. Bernstein, D. S., N. Buter, …, M. Wickens. 2002. Analyzing mRNA-protein complexes using a yeast three-hybrid system. *Methods.* 26:123–141.

28. Stumpf, C. R., L. Opperman, and M. Wickens. 2008. Chapter 14. Analysis of RNA-protein interactions using a yeast three-hybrid system. *Methods Enzymol.* 449:295–315.

29. Wilson, D. N., and K. H. Nierhaus. 2005. Ribosomal proteins in the spotlight. *Crit. Rev. Biochem. Mol. Biol.* 40:243–267.

30. Öhman, A., A. Rak, …, T. Härd. 2003. NMR structure of the ribosomal protein L23 from *Thermus thermophilus*. *J. Biomol. NMR.* 26:131–137.

31. Hsiao, C., T. K. Lenz, …, L. D. Williams. 2013. Molecular paleontology: a biochemical model of the ancestral ribosome. *Nucleic Acids Res.* 41:3373–3385.